Radiative transport theory for light propagation in luminescent media

Derya Şahin* and Boaz Ilan

School of Natural Sciences, University of California Merced, Merced, California 95343, USA
**Corresponding author: dsahin@ucmerced.edu*

Received November 30, 2012; revised February 26, 2013; accepted March 11, 2013;
posted March 15, 2013 (Doc. ID 180933); published April 8, 2013

We propose a generalization of radiative transport theory to account for light propagation in luminescent random media. This theory accounts accurately for the multiple absorption and reemission of light at different wavelengths and for anisotropic luminescence. To test this theory, we apply it to model light propagation in luminescent solar concentrators (LSCs). The source-iteration method is used in two spatial dimensions for LSCs based on semiconductor quantum dots and aligned nanorods. The LSC performance is studied in detail, including its dependence on particle concentration and the anisotropy of the luminescence. The computational results using this theory are compared with Monte Carlo simulations of photon transport and found to agree qualitatively. The proposed approach offers a deterministic methodology, which can be advantageous for analytic and computational modeling. This approach has potential for more efficient and cost-effective LSCs, as well as in other applications involving luminescent radiation.

OCIS codes: 030.5620, 260.3800, 290.4210, 220.1770, 350.6050.

1. INTRODUCTION

Radiative transport theory is a phenomenological approach for modeling the propagation and scattering of radiation through random media using the radiative transport equation (RTE) [1,2]. It has been applied successfully to many problems, such as neutron scattering, atmospheric scattering of light, and light propagation in tissue with application to medical imaging. With few exceptions (notably neutron scattering), radiative transport theory has been traditionally applied to **elastic** scattering, where the scattered radiation has the same energy as the incident one. However, when light is absorbed by luminescent particles and is reemitted, the reemitted wavelength (energy) differs from the absorbed one, i.e., luminescence is a form of **inelastic** scattering. This is the case, for example, for light propagation in luminescent solar concentrators (LSCs) and in tissue containing lumophores for luminescence optical tomography. When light propagates through such a medium, it can undergo multiple absorption and re-emission, which is detrimental for most applications.

In this study, we propose a generalization of radiative transport theory for modeling light propagation through a medium that contains luminescent scatters. We call the governing equation the luminescent RTE (LRTE). We apply this theory to model light propagation in LSCs. The measured data enter as parameters in the LRTE.

LSCs can capture sunlight over a large area using low-cost materials and redirect light onto a solar photovoltaic (PV) cell at the edge of the device [3,4] (see Fig. 1). The LSC contains luminescent particles that absorb sunlight and re-emit it at a longer wavelength, which can be in the PV bandgap. The main idea behind the design of LSCs is to reduce operational cost substantially by requiring a smaller amount of expensive PV material. In addition, unlike PVs, LSCs can also absorb diffuse light, thereby negating the need for any tracking mechanism. However, despite more than 30 years of research, LSCs are not yet commercially available, primarily due to their inefficiency (see [3–17] for recent studies of LSCs).

The development of LSCs faces several challenges. Two major challenges are increasing the re-emission of light (the photoluminescence quantum yield) while reducing the self-absorption, i.e., increasing the Stokes shift between the absorption and reemission spectra (see Fig. 2). Another challenge is decreasing the escape of light from the top surface of the LSC. Recently, it has been proposed to use aligned semiconductor (CdTe–CdSe) nanorods in LSCs to reduce these losses [13]. In this study, we use the LRTE approach to find the optimal particle concentration and the optimal LSC geometry for LSCs based on these semiconductor nanoparticles. Direct computations of the solutions of the LRTE are performed in two spatial dimensions using the source-iteration method [18]. Related problems have been studied recently using Monte Carlo simulations of "photon transport" [6,12,13,19,20]. The two approaches are compared in detail and found to agree qualitatively. In particular, they yield comparable optimal particle concentrations for LSC performance. These results show the accuracy and feasibility of the approach based on the deterministic LRTE. Another advantage of this methodology is that, as a deterministic equation, the LRTE lends itself naturally to detailed analytic modeling.

2. LUMINESCENT RADIATIVE TRANSPORT THEORY

The theory of radiative transfer/transport has been successful for describing scattering of light in random media, where the scattering is elastic, i.e., the scattered wavelength (which is inversely proportional to photon energy) is the same as the incident wavelength [1,2,21]. On the other hand, fluorescence and other luminescence effects are examples of inelastic

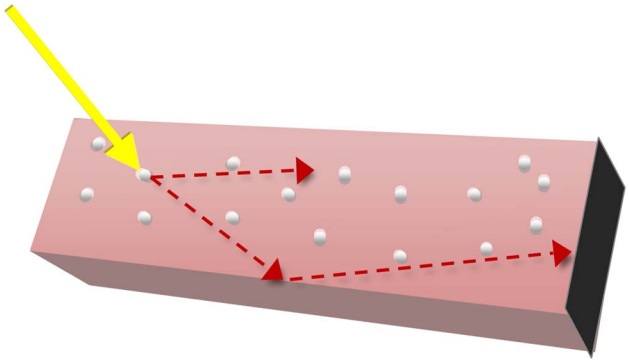

Fig. 1. (Color online) Illustration of light propagation in an LSC. Sunlight (solid arrow) is incident on the top surface, absorbed and reemitted by fluorescent nanoparticles (small spheres), and guided toward the PV cell on the right edge.

scattering, where the reemitted wavelength differs from the absorbed one. By analogy, it is reasonable to assume that light propagation in a random luminescent medium can be described by an extension of radiative transport theory. Such a theory would be useful in various areas of research, including solar science (see below) and fluorescence optical tomography [22]. However, very few studies have considered such models. We propose a radiative transport theory to model light propagation in luminescent media. Our approach begins with a general formalism and focuses on modeling LSCs.

The fundamental quantity in this theory is the radiance (or specific intensity), which is the power per projected surface area per unit direction per unit wavelength. In elastic scattering, the wavelength dependence of the radiance is usually suppressed. Here, this dependence is included explicitly and the radiance is denoted by

$$I(\mathbf{x},\Omega,\lambda,t):\mathcal{D}\times\mathbf{S}^2\times\Lambda\times[0,t_{\max}]\to\mathbb{R}\geq 0$$

with $\mathcal{D}\subset\mathbb{R}^3$ the spatial domain, $\mathbf{S}^2$ the unit sphere of directions, and Λ the set of wavelengths participating in the processes. In general, light propagation in random luminescent media can be described by a general LRTE,

$$\frac{1}{c}\frac{\partial I}{\partial t}+\Omega\cdot\nabla I+\mu_a\mathcal{L}_aI-\mu_r\mathcal{L}_rI=0, \tag{1}$$

where c is light speed, μ_a and μ_r are absorption and reemission constants (in [1/cm]), respectively, and $\mathcal{L}_a$, $\mathcal{L}_r$ are the corresponding absorption and reemission operators defined

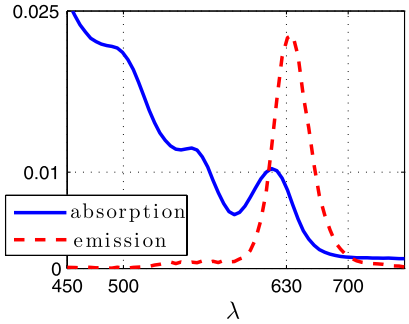

Fig. 2. (Color online) Normalized absorption and re-emission spectra [i.e., $f_a(\lambda)$ and $f_r(\lambda)$, respectively] corresponding to semiconductor CdSe–CdTe nanoparticles (from [13]).

below. To model the absorption operator, we recall the Beer–Lambert law, according to which the probability of absorption of light after a propagation distance Δs is

$$P_{\text{abs}}(\Delta s;\lambda)=1\text{–}10^{-\epsilon(\lambda)M\Delta s}, \tag{2}$$

where $\epsilon(\lambda)$ is the (dimensional) extinction coefficient (in [1/mol cm]) and M the molar concentration of the luminescent particles (in [mol/L]). The absorption constant μ_a is proportional to the molar concentration as (see also [23])

$$\mu_a=\ln(10)M\int_\Lambda\epsilon(\lambda)\mathrm{d}\lambda. \tag{3}$$

It is convenient to define the normalized absorption spectrum:

$$f_a(\lambda)=\frac{\epsilon(\lambda)}{\int_\Lambda\epsilon(\lambda)\mathrm{d}\lambda}. \tag{4}$$

Thus, $\int_\Lambda f_a(\lambda)\mathrm{d}\lambda=1$. Combining these definitions, the Beer–Lambert law of Eq. (2) is modeled by

$$\mathcal{L}_aI=f_a(\lambda)I. \tag{5}$$

In general, the re-emission operator in Eq. (1) can be written as

$$\mathcal{L}_rI=\int_\Lambda\int_{\mathbf{S}^2}K_r(\lambda,\lambda',\Omega,\Omega')I(\mathbf{x},\Omega',\lambda')\mathrm{d}\Omega'\mathrm{d}\lambda', \tag{6}$$

where $K_r(\lambda,\lambda',\Omega,\Omega')$ is a reemission kernel. The physical meaning of the reemission kernel is the probability that light that is absorbed in direction Ω' and wavelength λ' will be reemitted in direction Ω and wavelength λ. The (elastic scattering) RTE is a special case of the LRTE when the absorption and reemission spectra "coalesce" on the same single wavelength, i.e.,

$$K_r(\lambda,\lambda',\Omega,\Omega')=\delta(\lambda-\lambda')p_r(\Omega,\Omega'),$$

where δ is the Dirac delta function and $p_r(\Omega,\Omega')$ is the phase function. In that case, Eq. (1) reduces to the standard RTE:

$$\frac{1}{c}\frac{\partial I}{\partial t}+\Omega\cdot\nabla I=-\mu_aI+\mu_t\int_{\mathbf{S}^2}p_r(\Omega,\Omega')I(\mathbf{x},\Omega')\mathrm{d}\Omega',$$

where $\mu_t=\mu_a+\mu_s$ and μ_s is the scattering constant.

Let us consider light propagation in LSCs based on semiconductor particles. Since solar illumination on the LSC changes very slowly, time dependence can be neglected, leading to the time-independent LRTE:

$$\Omega\cdot\nabla I+\mu_af(\lambda)I-\mu_r\mathcal{L}_rI=0. \tag{7}$$

For LSCs based on semiconductor nanoparticles, such as CdSe–CdTe, the luminescence is approximately independent of the incident radiation [24]. To model this, we propose the "memoryless" anisotropic reemission phase function, $p_r(\Omega,\Omega';g)=p_r(\Omega;g)\delta(\Omega-\Omega')$, where g is an anisotropy parameter. Unlike the usual notion of anisotropy in radiative transport theory [2], $p_r(\Omega;g)$ depends on the absolute angle Ω

rather than $\Omega \cdot \Omega'$ for forward-scattering kernels. The corresponding reemission operator is

$$\mathcal{L}_r I = p_r(\Omega; g) f_r(\lambda) \int_{S^2} \int_{\Lambda} f_a(\lambda') I \mathrm{d}\Omega' \mathrm{d}\lambda', \tag{8}$$

where $f_r(\lambda)$ is the normalized re-emission spectrum [i.e., $\int_{\Lambda} f_r(\lambda)\mathrm{d}\lambda = 1$]. In fluorescent media, the quantum yield, QY, is the probability that a photon that is absorbed will be re-emitted (at any wavelength). Therefore, the absorption and re-emission constants are related by

$$\mu_r = \mathrm{QY}\mu_a. \tag{9}$$

The physical meaning of the re-emission operator of Eq. (8) is that the total absorbed light power, i.e., the double integral on the right-hand side of Eq. (8), is reemitted at wavelengths in accordance with the re-emission spectrum, $f_r(\lambda)$.

Recently, Yudovsky and Pilon proposed two coupled RTEs to model fluorescence imaging [25] (see also [26–28] for related studies within the diffusion approximation). We also note that RTEs with general kernels of the type in Eq. (6) have been proposed for modeling luminescence for computer graphics applications [29–31]. The main advantage of Eqs. (7)–(9) is that they depends only on physically measurable quantities, i.e., the absorption and re-emission spectra, the absorption constant [or, by Eq. (3), the molar concentration], and the quantum yield. Moreover, this theory allows for modeling accurately the phenomenon of self-absorption, i.e., light that has been reemitted can be reabsorbed. Self-absorption is due to the overlap of the absorption and reemission spectra (Fig. 2) and sets a fundamental limitation on the performance of LSCs.

To solve Eq. (7), the boundary conditions must be specified in a well-posed manner. On the boundary of a LSC, the conditions can be written as

$$\begin{aligned} I &= S_b + RI \quad \text{on } \Gamma_{in}, \\ \Gamma_{in} &= \{(\mathbf{x}, \Omega, \lambda) \in \partial D \times \mathbf{S}^2 \times \Lambda, \Omega \cdot \nu < 0\}, \end{aligned} \tag{10}$$

where $\partial\mathcal{D}$ is the spatial boundary of the LSC, ν is the unit outward normal, R is the reflection coefficient, and S_b is the incident radiance. These conditions prescribe the radiance at the spatial boundary for all directions pointing into the domain.

Analytical solutions of Eq. (7) can only be found in special cases. In this study, solutions of this boundary value problem are computed using numerical methods. For simplicity, we assume below that the LSC is infinite in extent in the y direction, so that only one angular variable is needed. As we shall see, the 2D results are qualitatively similar to 3D results for the same setup obtained using Monte Carlo simulations [13]. Therefore, we consider a rectangular LSC, such that x and z are the horizontal and vertical spatial variables on the LSC's edge surface, respectively, and $\varphi \in [0, 2\pi)$ is the angular variable ($\varphi = 0$ along the positive x axis). In this case, the radiance $I(x, z, \varphi, \lambda)$ is measured in units of [W/cm sr nm]. The LRTE [Eq. (7)] reduces to

$$\begin{aligned} &\cos\varphi \frac{\partial I}{\partial x} + \sin\varphi \frac{\partial I}{\partial z} + \mu_a f_a(\lambda) I \\ &- \mu_r f_r(\lambda) p_r(\varphi; g) \int_0^{2\pi} \int_{\Lambda} f_a(\lambda') I \mathrm{d}\varphi' \mathrm{d}\lambda' = 0. \end{aligned} \tag{11}$$

We consider two kinds of particles: spherical CdSe–CdTe quantum dots, which reemit isotropically ($g = 0$ below), and heterojunction CdSe–CdTe nanorods. The nanorods are assumed to absorb light isotropically and luminesce in a preferred direction orthogonal to the long axis [32]. Assuming these nanorods can be aligned in the LSC (e.g., in a liquid crystal matrix) with their long axes perpendicular to the top surface, the luminescence is preferentially in the direction parallel to the top surface. This is designed to reduce the escape of light from the top surface [13] (see corresponding 3D illustration in Fig. 3).

To model this anisotropic luminescence, we use the Henyey–Greenstein reemission function [33] (see Fig. 4):

$$p_r(\varphi; g) = \frac{1}{2\pi} \frac{1 - g^2}{1 - 2g\cos 2\varphi + g^2}. \tag{12}$$

For spherical quantum dots, $g = 0$ and $p_r = (2\pi)^{-1}$ is isotropic. In the idealized limiting case, the luminescence would be only in the direction parallel to the top surface. This corresponds to $g \to 1$ and $\lim_{g\to 1} p_r(\varphi; g) = \delta(\cos 2\varphi - 1)$. However, the nanorods cannot be perfectly aligned and cannot luminesce exactly in this way. Therefore, a more realistic case is to consider $0 < g < 1$, which serves to model nanorods that are not ideal in this sense. Thus, for any $0 < g < 1$, Eq. (12) describes luminescence in a cone centered about the x axis, whose opening angle decreases monotonically as g approaches 1 (in the 3D case this corresponds to conical luminescence centered about the x–y plane).

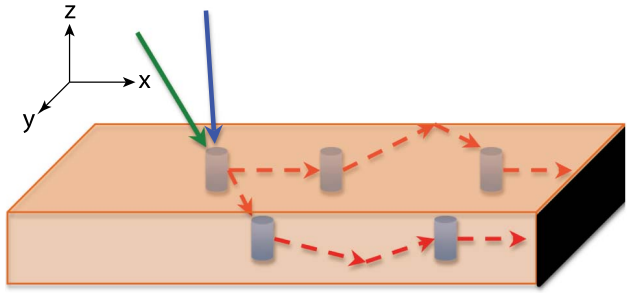

Fig. 3. (Color online) Illustration of light propagation in a 3D LSC based on anisotropic nanorods. A PV cell is located at the right edge. Perfect mirrors are assumed to cover the bottom surface and all the other edges.

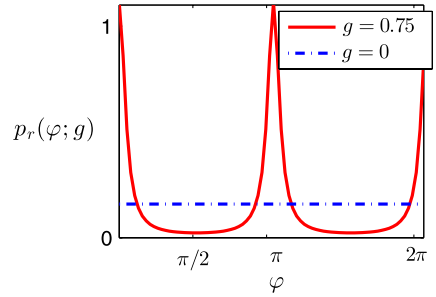

Fig. 4. (Color online) Dependence of the reemission phase function in Eq. (12) on the polar angle φ for isotropic quantum dots ($g = 0$, dotted–dashed line) and aligned nanorods ($g = 0.75$, solid curve). The nanorods luminesce preferentially along the x axis, i.e., $\varphi = 0$ and $\varphi = \pi$.

We now consider a box-shaped LSC of length l_x, $x \in [-(l_x/2),(l_x/2)]$ and thickness (or height) l_z, $z \in [-(l_z/2),(l_z/2)]$. The solar PV cell covers the right side $x=(l_x/2)$. We assume the PV absorbs all the light that impinges on it. This can be modeled using the "vacuum" boundary conditions:

$$I\left(\frac{l_x}{2},z,\varphi,\lambda\right)=0, \qquad \varphi\in\left(\frac{\pi}{2},\frac{3\pi}{2}\right). \tag{13}$$

The bottom surface and the left edge surface are assumed to be covered by perfect mirrors. The associated boundary conditions are

$$I\left(-\frac{l_x}{2},z,\varphi,\lambda\right)=I\left(-\frac{l_x}{2},z,\pi+\varphi,\lambda\right), \quad \varphi\in\left(-\frac{\pi}{2},\frac{\pi}{2}\right), \tag{14}$$

$$I\left(x,-\frac{l_z}{2},\varphi,\lambda\right)=I\left(x,-\frac{l_z}{2},2\pi-\varphi,\lambda\right), \quad \varphi\in(\pi,2\pi). \tag{15}$$

At the top surface light is partially reflected and we use the Fresnel reflection coefficient $R(\varphi)$ for unpolarized light [34] as

$$I\left(x,\frac{l_z}{2},\varphi,\lambda\right)=[1-R(\varphi)]I\left(x,\frac{l_z}{2},\varphi,\lambda\right)+R(\varphi')I\left(x,\frac{l_z}{2},\varphi',\lambda\right), \tag{16}$$

where $\varphi'=2\pi-\varphi$ is the reflected angle. We assume that the solar illumination on the top surface of the LSC is spatially uniform and centered at normal incidence $\varphi=3\pi/2$, i.e.,

$$S_b(\varphi,\lambda)=f_{\mathrm{sol}}(\lambda)e^{-8\left(\varphi-\frac{3\pi}{2}\right)^2}, \qquad \varphi\in(\pi,2\pi), \tag{17}$$

where $f_{\mathrm{sol}}(\lambda)$ is the solar irradiance measured at sea level [35].

We solve the boundary value problem of Eqs. (11)–(17) using the source-iteration method [36] and an upwinding numerical scheme [18]). The source-iteration method is an efficacious approach for solving boundary value problems that involve large linear systems. To use it, the discretized radiance is denoted as $I_{i,j,m,k}$, where (i,j,m,k) are the indices corresponding to (x,z,φ,λ) and the number of corresponding grid points are $(N_x,N_z,N_\varphi,N_\lambda)$. We seek an iterative solution as

$$I(x,z,\varphi,\lambda)\approx I_{i,j,m,k}\approx\sum_{s=0}^{\mathrm{maxiter}} I^{(s)}_{i,j,m,k},$$

where maxiter denotes the number of iterations for the solution to converge. As a stopping criterion, we use

$$\|I^{(s)}(x,z,\varphi,\lambda)\|_\infty=\max_{i,j,m,k}|I^{(s)}_{i,j,m,k}|\le\Delta$$

within a fixed tolerance of $\Delta=10^{-5}$. The source-iteration method converges rapidly after relatively few iterations. For example, choosing the physical constants as $l_x=3$[cm], $l_z=0.4$[cm], $\mu_a=600$[1/cm], QY $=0.95$, and anisotropy parameter $g=0.75$, and the numerical grid sizes as $N_x=48$, $N_z=6$, $N_\varphi=80$, and $N_\lambda=14$, the solution converges within 250 iterations (see Fig. 5).

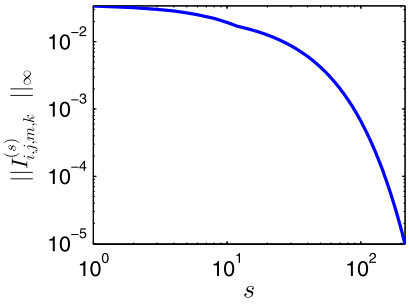

Fig. 5. (Color online) Convergence of the LRTE solution as a function of iteration number (loglog plot).

3. LSC PERFORMANCE METRICS

There are three kinds of loss mechanisms of light in LSCs [5,9–11,15,17].

1. Reemission losses. Light that is absorbed is not necessarily reemitted. This is captured by the quantum yield, QY.
2. Self-absorption losses. Light that is reemitted can be reabsorbed (self-absorption). In general, light can undergo multiple absorption and reemission events, which reduces its intensity inside the LSC. Self-absorption is due to the overlap of the absorption and reemission spectra (see Fig. 2). Thus, self-absorption is determined primarily by the quantum yield and the absorption and reemission spectra.
3. Escape losses. Light can escape from the top surface of the LSC.

We refer to the combination of the reemission and self-absorption losses as "combined absorption losses."

Our goal is to optimize the experimentally controllable LSC design parameters, so as to minimize these losses and, therefore, maximize the light that reaches the PV. To this end, we assume that the absorption and reemission spectra are fixed as shown in Fig. 2 and that the quantum yield is fixed as QY $=0.95$. These are measured values for CdSe–CdTe semiconductor particles [13]. We assume that the **controllable LSC design parameters** are

1. the absorption constant, μ_a, or, equivalently by Eq. (3), the molar concentration of the particles;
2. the LSC size, i.e., the thickness l_z and length l_x; and
3. the anisotropy factor g of the aligned nanorods.

An often used LSC performance metric is the "optical efficiency," which is the ratio of the spectral power at a particular wavelength collected by the PV cell to the solar spectral power at a particular wavelength that is incident on the top surface, i.e.,

$$\eta_{\mathrm{pv}}(\lambda)=\frac{\Phi_{\mathrm{pv}}(\lambda)}{\Phi_{\mathrm{sol}}(\lambda)}, \tag{18}$$

where

$$\Phi_{\mathrm{pv}}(\lambda)=\int_{-\frac{l_z}{2}}^{\frac{l_z}{2}}\int_{-\frac{\pi}{2}}^{\frac{\pi}{2}} I\left(\frac{l_x}{2},z,\varphi,\lambda\right)\mathrm{d}\varphi\mathrm{d}z,$$

Φ_{pv} denotes the spectral power at a particular wavelength at the PV edge in [W/nm]. Φ_{sol} is the solar spectral power at a particular wavelength at the LSC's top surface in [W/nm], and

$$\Phi_{\mathrm{sol}}(\lambda) = l_x \int_{\pi}^{2\pi} S_b(\varphi, \lambda) \mathrm{d}\varphi.$$

Using Eq. (17),

$$\Phi_{\mathrm{sol}}(\lambda) = C l_x f_{\mathrm{sol}}(\lambda), \qquad C \approx 0.62.$$

We define the wavelength-averaged optical efficiency,

$$\bar{\eta}_{\mathrm{pv}} = \frac{\int_{\Lambda} \eta_{\mathrm{pv}}(\lambda) \mathrm{d}\lambda}{\int_{\Lambda} \Phi_{\mathrm{sol}}(\lambda) \mathrm{d}\lambda}, \tag{19}$$

and wavelength-averaged losses due to escape from the top surface,

$$\bar{\eta}_{\mathrm{top}} = \frac{\int_{\Lambda} \Phi_{\mathrm{top}}(\lambda) \mathrm{d}\lambda}{\int_{\Lambda} \Phi_{\mathrm{sol}}(\lambda) \mathrm{d}\lambda}, \tag{20}$$

where the spectral power at a particular wavelength that escapes from the LSC is

$$\Phi_{\mathrm{top}}(\lambda) = \int_{-\frac{l_x}{2}}^{\frac{l_x}{2}} \int_{0}^{\pi} [1 - R(\varphi)] I\left(x, \frac{l_z}{2}, \varphi, \lambda\right) \mathrm{d}\varphi \mathrm{d}x, \tag{21}$$

where $[1 - R(\varphi)]$ is the fraction of the reemitted light that is transmitted outside the LSC [3]. Since light is either collected by the PV, escapes from the top surface, or combined absorption losses, the wavelength-averaged combined absorption loss is

$$\bar{\eta}_{\mathrm{abs}} = 1 - \bar{\eta}_{\mathrm{pv}} - \bar{\eta}_{\mathrm{top}}. \tag{22}$$

Finally, as discussed in Subsection 4.A.3, another useful metric for the LSC performance is the LSC optical gain [13]:

$$\bar{\Gamma} = \bar{\eta}_{\mathrm{pv}} \times G, \qquad G \doteq \frac{A_{\mathrm{top}}}{A_{\mathrm{pv}}} \doteq \frac{l_x}{l_z}, \tag{23}$$

where G is often called the geometric gain factor, A_{top} is the top surface area, and A_{pv} is the area covered by the PV cell.

4. COMPUTATIONAL RESULTS

To make detailed computations for the semiconductor LSC performance, we solve the boundary value problem in Eqs. (11)–(17) for particular LSC design parameters, i.e., QY = 0.95 and $l_z = 0.4$[cm]. The refractive index of the LSC waveguide is taken as $n_{\mathrm{LSC}} = 1.7$. From Snell's law, light is captured in the LSC whenever the reemitted polar angle is greater than 36°. We seek the optimal design parameters mentioned above, i.e., μ_a and G.

A. Optimal LSC Design Parameters

1. Optimal Absorption Constant

To optimize the LSC design parameters, at first we seek the optimal absorption constant, μ_a. Here we use $g = 0.75$. Figure 6 shows the wavelength-averaged optical efficiency and loss mechanisms as functions of μ_a. At low particle concentrations ($\mu_a < 100$[1/cm]), much of the incident light is lost due to top loss. Since the light is incident at normal angle, most of the light escapes from the LSC's top surface. At low particle concentration, as seen in Fig. 6, a small amount of light is either collected or lost due to self-absorption.

It is well known that numerical solutions of the RTE tend to have different characteristics for weak scattering media and localized sources [36]. This is due, in part, to the angular discretization leading to the "ray effects" [37], in the weakly scattering regime, i.e., for small μ_a, and when the source is collimated. In this regime, the source-iteration method becomes highly sensitive to the angular discretization. The ray effects are implicitly included in the combined absorption loss [Eq. (22)]. This explains why the absorption loss does not vanish at low particle concentrations. On the other hand, ray effects are mitigated in the strongly scattering regime, i.e., for large μ_a. In the intermediate regime, Fig. 6 shows that the optical efficiency has a maximum value, $\max_{\mu_a}(\bar{\eta}_{\mathrm{pv}}) \approx 0.3$, obtained at $\mu_{\mathrm{opt}} \approx 600$[1/cm]. At this optimal value, the absorption losses are somewhat large and the escape from the top surface is quite small. Hence, the optimal absorption constant is obtained from a balance between these competing loss mechanisms.

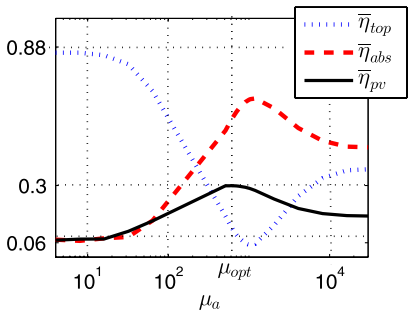

Fig. 6. (Color online) Wavelength-averaged optical efficiency [Eq. (19) (solid)], the averaged escape losses from the top surface [Eq. (20), dots], and the combined absorption losses [Eq. (22), dashes], as functions of the absorption constant, μ_a (in [1/cm]) using aligned nanorods ($g = 0.75$).

2. Effect of Anisotropy

We now seek to study the effect of anisotropy of the luminescence on the LSC performance. We use the previously given LSC dimensions, $\mu_a = 600$, and vary the anisotropy factor, g, in the reemission function [Eq. (12)]. Figure 7 shows that the LSC performance increases monotonically with g. In particular, in the ideal case of $g = 1$, when light is reemitted only in the $\pm x$ directions, the LSC optical gain is 30% greater than using isotropic quantum dots. This suggests that aligning the nanorods can have a significant impact on the LSC performance.

3. Optimal LSC Length

To optimize the LSC's length using the concept of geometric gain factor [see Eq. (23)], the idea is to make the area covered

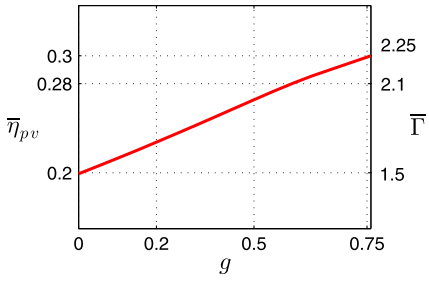

Fig. 7. (Color online) Wavelength-averaged optical efficiency (left axis) and LSC optical gain (right axis) as functions of the anisotropy factor.

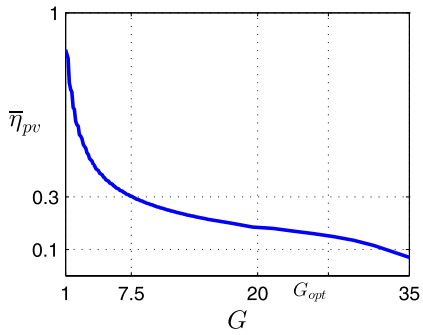

Fig. 8. (Color online) Wavelength-averaged optical efficiency with $\mu_a = 600$ and $g = 0.75$ as a function of the geometric gain factor $G = (l_x/l_z)$ with $l_z = 0.4$[cm].

by the PV cell constant, while the top surface area is varied. To do this, we use $\mu_a = 600$[1/cm], the anisotropy factor $g = 0.75$, and vary the length l_x, while fixing the thickness at $l_z = 0.4$[cm]. The results in Fig. 8 show that the optical efficiency decreases as the length l_x increases. This makes sense, because as l_x increases, light has to travel a longer distance to reach the PV, thus increasing the losses due to escape from the top surface and self-absorption. However, the optical efficiency is not the right metric for predicting the LSC's performance, because it is based on power rather than power density.

Figure 9 shows that the optimal geometric gain factor is $G_{\text{opt}} \approx 27$, which corresponds to $l_x \leq 10.8$[cm]. Thus, the optimal LSC design is fairly thin (in z) and long (in x). Furthermore, the maximal LSC optical gain is $\bar{\Gamma}^{\max} \approx 4$. While this is an idealized 2D scenario, it is nonetheless encouraging for using aligned nanorods.

5. MONTE CARLO METHOD FOR LIGHT PROPAGATION IN LSCS

A. Method

Monte Carlo (MC) simulations for photon transport are a common tool for studying light propagation in random media. They have been extensively used to model light propagation in several multiphysics problems [19,38]. One of the recent application areas is LSCs [5,6,12,13]. To compare with the above LRTE results, we use a 2D version of the MC algorithm in [13]. We assume that light is normally incident on the top surface, use the "particles" as above, i.e., same absorption and reemission spectra, QY = 0.95, $g = 0.75$, and use the same boundary conditions as above.

Briefly, to obtain accurate results, a photon packet of 10^7 photons (or discrete particles), whose wavelengths are sampled from the solar spectrum, are incident on the top surface uniformly in x. Each photon is tracked until either collected at the PV or lost. The probability of absorption is calculated using Eq. (2). Specifically, in order to accelerate the MC computations [5,6,13], the probability that a photon entering the LSC at normal incidence is initially absorbed is computed as

$$\xi \leq P_{\text{abs}}(2l_z, \lambda_i), \tag{24}$$

where λ_i is the incident wavelength and ξ is a uniform random variable in (0, 1). When Eq. (24) is not satisfied, the incident photon is assumed not to be captured inside the LSC. If a photon is initially captured in the LSC, its reemission probability is the quantum yield, QY. If reemitted, the photon's wavelength, direction, and position are updated as follows. The reemitted wavelength is sampled from $f_r(\lambda)$. The direction of the reemitted photon is found from the accumulated distribution function Θ obtained from Eq. (12), i.e.,

$$P(\varphi; g) = \frac{1}{2\pi}\begin{cases} \Theta(\varphi; g), & \varphi \in [0, \pi/2), \\ \pi + \Theta(\varphi; g), & \varphi \in [\pi/2, 3\pi/2), \\ 2\pi + \Theta(\varphi; g), & \varphi \in [3\pi/2, 2\pi), \end{cases} \tag{25}$$

where

$$\Theta(\varphi; g) = \tan^{-1}(\tilde{g}\,\tan\,\varphi), \qquad \tilde{g} = \frac{1-g}{1+g}.$$

Inverting Eq. (25), the reemission angle is computed as

$$\varphi = \begin{cases} \tan^{-1}[\tilde{g}\,\tan(2\pi\xi)], & \xi \in [0, 1/4); \\ \tan^{-1}[\tilde{g}\,\tan(\pi(2\xi - 1))], & \xi \in [1/4, 3/4); \\ \tan^{-1}[\tilde{g}\,\tan(2\pi(\xi - 1))], & \xi \in [3/4, 1), \end{cases}$$

where ξ is a uniformly random variable in (0, 1). The photon's position is then updated using

$$x' = x + \Delta s\,\cos\,\varphi, \qquad z' = z + \Delta s\,\sin\,\varphi,$$

where Δs is found by inverting the Beer–Lambert law [Eq. (2)] as

$$\Delta s = -\frac{1}{\epsilon(\lambda)M}\log_{10}\xi,$$

where ξ is a random variable uniformly distributed in (0, 1). If the photon reaches the PV cell at $x = (l_x/2)$, it is assumed to be collected. The LSC performance metrics are computed similarly to Eqs. (18)–(23) (see [13] for further details of this algorithm).

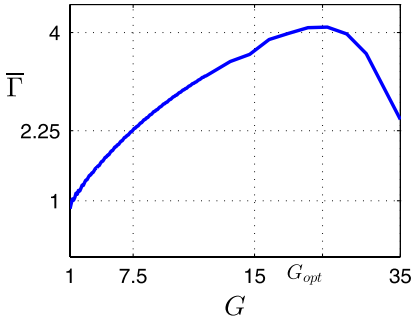

Fig. 9. (Color online) LSC optical gain for the same parameters as in Fig. 8.

B. Comparison of LRTE and Monte Carlo Approaches

Using the MC method outlined above and the same LSC size $l_x = 3$[cm] $l_z = 0.4$[cm] and anisotropy factor $g = 0.75$, the wavelength-averaged optical efficiency [Eq. (19)] is computed while varying the absorption constant, μ_a. To compare the results with the LRTE computations, we use Eq. (3). Figure 10 shows that the optimal absorption constants are almost the same using the LRTE and MC approaches ($M_{\text{opt}} \approx 2.6 \times 10^{-6}$[mol/L], $\mu_{\text{opt}} \approx 600$). Furthermore, the maximal optical efficiency is also approximately the same as found using the LRTE approach, i.e., $\bar{\eta}_{\text{pv}} \approx 0.3$. This shows the consistency between the deterministic LRTE and the statistical MC approaches.

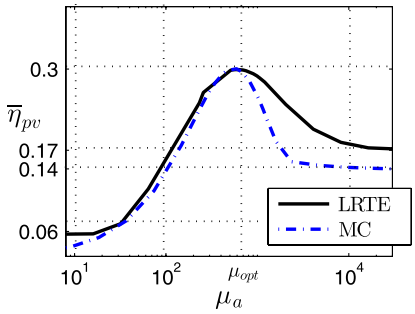

Fig. 10. (Color online) Wavelength-averaged optical efficiency as a function of the absorption constant obtained using the LRTE (solid) and MC (dashes).

C. Discussion

We do not make the claim that the deterministic approach is better than the statistical one. However, they complement each other. The MC approach is conceptually simpler, easier to code, and has certain numerical advantages when dealing with highly collimated sources, a weak scattering regime, and in many dimensions. On the other hand, deterministic computational techniques for the standard RTE are quite efficient and are also commonly used in the literature to model real-world problems [18,39]. While the LRTE has an additional dimension compared with the standard RTE, this study shows that the LRTE can be solved computationally by adapting existing numerical methods. The agreement between the approaches serves to validate each other (see [40] for a rigorous comparison between these approaches). Another benefit of the LRTE is that it is amenable to further analytical modeling, i.e., rigorous mathematical techniques and asymptotics. Further studies are required to make this approach more realistic, i.e., model a 3D LSC, include polarization effects, etc.

6. CONCLUSIONS

This study highlights the role of radiative transport theory in modeling light propagation in luminescent media. In particular, we have developed a deterministic approach using the LRTE [Eq. (7)] that takes into account accurately absorption, self-absorption, and anisotropic luminescence. Using the LRTE in two spatial dimensions, the optimal LSC design parameters are computed and the results using aligned nanorods are encouraging for the LSC technology. This yields accurate and insightful results for designing LSCs. Furthermore, the LRTE approach can be extended to model other multidimensional problems involving luminescence radiation.

ACKNOWLEDGMENTS

This research is supported by the Natural Science Foundation SOLAR Program under Grant No. CHE-0934615. The authors thank the anonymous reviewers for their helpful comments. D. Şahin would like to thank N. Kumar for valuable discussions on the implementation of the Monte Carlo algorithm.

REFERENCES

1. S. Chandrasekhar, *Radiative Transfer* (Dover, 1960).
2. A. Ishimaru, *Wave Propagation and Scattering in Random Media* (Wiley-IEEE, 1999).
3. J. S. Batchelder, A. H. Zewail, and T. Cole, "Luminescent solar concentrators. 1: theory of operation and techniques for performance evaluation," Appl. Opt. **18**, 3090–3110 (1979).
4. M. S. de Cardona, M. Carrascosa, F. Meseguer, F. Cusso, and F. Jaque, "Outdoor evaluation of luminescent solar concentrator prototypes," Appl. Opt. **20**, 2934–2940 (1985).
5. R. W. Olson, F. L. Roger, and M. D. Fayer, "Luminescent solar concentrators and the reabsorption problem," Appl. Opt. **20**, 2934–2940 (1981).
6. V. Sholin, J. D. Olson, and S. A. Carter, "Semiconducting polymers and quantum dots in luminescent solar concentrators for solar energy harvesting," J. Appl. Phys. **101**, 123114 (2007).
7. M. J. Currie, J. K. Mapel, T. D. Heidel, S. Goffri, and M. A. Baldo, "High-efficiency organic solar concentrators for photovoltaics," Science **321**, 226–228 (2008).
8. L. H. Slooff, E. E. Bende, A. R. Burgers, T. Budel, M. Pravettoni, R. P. Kenny, E. D. Dunlop, and A. Büchtemann, "A luminescent solar concentrator with 7.1% power conversion efficiency," Phys. Status Solidi RRL **2**, 257–259 (2008).
9. P. P. C. Verbunt, A. Kaiser, K. Hermans, C. W. M. Bastiaansen, D. J. Broer, and M. G. Debije, "Controlling light emission in luminescent solar concentrators through use of dye molecules aligned in a planar manner by liquid crystals," Adv. Funct. Mater. **19**, 2714–2719 (2009).
10. S. Tsoi, D. J. Broer, C. W. Bastiaansen, and M. G. Debije, "Patterned dye structures limit reabsorption in luminescent solar concentrators," Opt. Express **18**, A536–A543 (2010).
11. C. L. Mulder, P. D. Reusswig, A. M. Velázquez, H. Kim, C. Rotschild, and M. A. Baldo, "Dye alignment in luminescent solar concentrators: I. Vertical alignment for improved waveguide coupling," Opt. Express **18**, A79–A90 (2010).
12. S. McDowall, B. L. Johnson, and D. L. Patrick, "Simulations of luminescent solar concentrators: effects of polarization and fluorophore alignment," J. Appl. Phys. **108**, 053508 (2010).
13. D. Şahin, B. Ilan, and D. Kelley, "Monte-Carlo simulations of light scattering in luminescent solar concentrators based on semiconductor nanoparticles," J. Appl. Phys **110**, 1–8 (2011).
14. R. H. Inman, G. V. Scherbatyuk, D. Medvedko, A. Gopinathan, and S. Ghosh, "Cylindrical luminescent solar concentrators with near-infrared quantum dots," Opt. Express **19**, 24308–24313 (2011).
15. F. Purcell-Milton and Y. K. Gun'ko, "Quantum dots for luminescent solar concentrators," J. Mater. Chem. **22**, 16687–16697 (2012).
16. H. Hernandez-Noyola, D. H. Potterveld, R. J. Holt, and S. B. Darling, "Optimizing luminescent solar concentrator design," Energy Environ. Sci. **5**, 5798–5802 (2012).
17. P. P. C. Verbunt, S. Tsoi, M. G. Debije, D. J. Broer, C. W. Bastiaansen, C.-W. Lin, and D. K. G. de Boer, "Increased efficiency of luminescent solar concentrators after application of organic wavelength selective mirrors," Opt. Express **20**, A655–A668 (2012).
18. H. Gao and H. Zhao, "A fast forward solver of radiative transfer equation," Transp. Theory Stat. Phys. **38**, 149–192 (2009).
19. S. A. Prahl, M. Keizer, S. L. Jacques, and A. J. Welch, "A Monte Carlo model of light propagation in tissue," in *SPIE Proceedings of Dosimetry of Laser Radiation in Medicine and Biology*, Vol. **IS(5)**, SPIE Institute Series (SPIE, 1989), pp. 102–111.
20. L. Wang, S. L. Jacques, and L. Zheng, "Monte Carlo modeling of photon transport in multi-layered tissues," Comput. Methods Programs Biomed. **47**, 131–146 (1995).
21. K. M. Case and P. F. Zweifel, *Linear Transport Theory* (Addison-Wesley, 1967).
22. J. Bertolotti, E. G. van Putten, C. Blum, A. Lagendijk, W. L. Vos, and A. P. Mosk, "Non-invasive imaging through opaque scattering layers," Nature **491**, 232–234 (2012).
23. W. W. Yu, L. Qu, W. Guo, and X. Peng, "Experimental determination of extinction coefficient of CdTe, CdSe, and CdS nanocrystals," Chem. Matter **15**, 2854–2860 (2003).
24. A. Chatten, K. Barnham, B. Buxton, N. Ekins-Daukes, and M. Malik, "Quantum dot solar concentrators," Semiconductors **38**, 909–917 (2004).
25. D. Yudovsky and L. Pilon, "Modeling the local excitation fluence rate and fluorescence emission in absorbing and strongly scattering multilayered media," Appl. Opt. **49**, 6072–6084 (2010).
26. G. Y. Panasyuk, Z.-M. Wang, J. C. Schotland, and V. A. Markel, "Fluorescent optical tomography with large data sets," Opt. Lett. **33**, 1744–1746 (2008).

27. A. D. Zacharopoulos, P. Svenmarker, J. Axelsson, M. Schweiger, S. R. Arridge, and S. Andersson-Engels, "A matrix-free algorithm for multiple wavelength fluorescence tomography," Appl. Phys. Lett. **17**, 3042–3051 (2009).
28. C. T. Xu, J. Axelsson, and S. Andersson-Engels, "Fluorescence diffuse optical tomography using upconverting nanoparticles," Appl. Phys. Lett. **94**, 251107 (2009).
29. J. T. Kajiya, "The rendering equation," Comput. Graph. **20**, 143–150 (1986).
30. A. S. Glassner, *Principles of Digital Images Synthesis* (Morgan Kaufmann, 1995).
31. H. W. Jensen, *Realistic Image Synthesis Using Photon Mapping* (AK Peters, 2001).
32. D. D. Cooke and M. Kerker, "Light scattering from long thin glass cylinders at oblique incidence," J. Opt. Soc. Am. **59**, 43–49 (1969).
33. J. G. Henyey and J. L. Greenstein, "Diffuse radiation in the galaxy," J. Astrophys. **93**, 70–83 (1941).
34. E. Hecht, *Optics* (Addison-Wesley, 1987).
35. K. Emery, "Reference solar spectral irradiance: air mass 1.5," Tech. Rep. (ASTM, 2000), http://rredc.nrel.gov/solar/spectra/am1.5.
36. E. E. Lewis and W. F. J. Miller, *Computational Methods of Neutron Transport* (Wiley, 1984).
37. K. D. Lathrop, "Ray effects in discrete ordinates equations," Nucl. Sci. Eng. **32**, 357–369 (1968).
38. L. Wang and H. Wu, *Biomedical Optics: Principles and Imaging* (Wiley, 2007).
39. A. D. Kim and M. Moscoso, "Radiative transfer computations for optical beams," J. Comput. Phys. **185**, 50–60 (2003).
40. G. Bal and O. Pinaud, "Accuracy of transport models for waves in random media," Wave Motion **43**, 561–578 (2006).